

1 **The Benefits of Continuous Local Regression for Quantifying Global Warming**

2

3 **David C. Clarke¹, Mark Richardson^{2,3}**

4

5 ¹Independent Researcher, Montreal, Quebec, Canada

6 ²Jet Propulsion Laboratory, California Institute of Technology, USA

7 ³Colorado State University, Fort Collins, USA

8

9 Corresponding author: David C. Clarke (dave@daveclarke.ca)

10 **Key Points:**

- 11
- 12 • Continuous local regression is an alternative to traditional IPCC temperature change estimation methods.
 - 13 • Global warming from near-global land-ocean observational series reached 1.14°C
 - 14 (likely range 1.05—1.25°C) in 2019 relative to 1850-1900.
 - 15 • Global surface air temperature reached 1.21°C (likely range 1.11—1.32°C), for a
 - 16 remaining 1.5°C carbon budget of ~220 GtCO₂ from 2020 on.

17 Abstract

18

19 Change in global mean surface temperature (ΔGMST) is a widely cited climate change indicator
20 that figures prominently in IPCC reports, in which it was estimated via linear regression or
21 differences between decade-plus period means. The Paris Agreement aims to limit warming
22 since preindustrial (here approximated as 1850—1900) to “well below” 2 °C, and by knowing
23 current ΔGMST it is possible to determine the remaining target-consistent warming and therefore
24 a relevant remaining carbon budget. We propose non-linear continuous local regression (LOESS)
25 using 40-year windows as a single method to derive ΔGMST with statistical uncertainty across
26 all periods of interest. Using the three datasets with almost complete spatial coverage since the
27 1950s, we evaluate 1850—1900 to 2019 ΔGMST as 1.14 °C with likely (17—83 %) range of
28 1.05—1.25 °C, based on combined statistical and observational uncertainty, compared with
29 1880—2019 linear regression of 1.03 °C using all five operational datasets. In two model large
30 ensembles LOESS, like period mean differences, is unbiased but provides a statistical error and
31 gives warming through 2019, rather than a 2010—2019 average centred at the end of 2014. We
32 compare observational and CMIP6 ΔGMST and estimate historical global surface air
33 temperature change (ΔGSAT) using the CMIP6 $\Delta\text{GSAT}/\Delta\text{GMST}$ ratio and its ensemble spread.
34 Finally, we calculate remaining carbon budgets given our ΔGSAT of 1.21 °C with likely range of
35 1.11—1.32 °C. We argue that continuous non-linear trend estimation offers substantial
36 advantages for assessment of long-term observational ΔGMST .

37 1 Introduction

38 Estimates of global mean surface temperature anomalies (GMST) and derived trends or changes,
39 ΔGMST , have featured prominently in IPCC reports, and are a key component in assessments of
40 climate change attribution (Bindoff et al., 2013), climate model validation (Flato et al., 2013),
41 global carbon budgets (Rogelj et al., 2018) and climate impacts (Hoegh-Guldberg et al., 2018).
42 Perhaps most importantly, the IPCC’s long-term ΔGMST estimate of 0.85°C, based on the 1880-
43 2012 linear trend, was a key scientific input to the Paris agreement to keep global surface
44 temperature change well below 2°C (IPCC, 2014; UNFCCC, 2015).

45

46 The IPCC Fifth Assessment Report (IPCC AR5; Hartmann et al., 2013a) used three GMST
47 datasets: HadCRUT4 (Morice et al., 2012), NASA GISTEMP (Hansen et al., 2010) and NOAA
48 MLOST (Vose et al., 2010). While HadCRUT4 begins in 1850, the NOAA and NASA datasets
49 began in 1880 and the 1880—2012 ordinary least squares (OLS) linear trend was a “headline”
50 warming estimate along with the HadCRUT4 1850—1900 to 2003—2012 difference. OLS
51 trends for all datasets were also given for 1951-2012 and 1979-2012 with uncertainties adjusted
52 to account for autocorrelated residuals (Santer et al., 2008; Hartmann et al., 2013b).

53

54 The IPCC Special Report on Global Warming of 1.5°C (IPCC SR1.5; Allen et al., 2018)
55 included two new GMST datasets that incorporated sophisticated spatial interpolation: Cowtan-
56 Way (Cowtan and Way, 2014a; Cowtan and Way, 2014b; Cowtan et al., 2015) and Berkeley
57 Earth (Rohde et al., 2011). Reported ΔGMST was $0.87 \pm 0.12^\circ\text{C}$ based on the average of
58 HadCRUT4, NOAA, NASA and Cowtan-Way. An observation based estimate of Global Surface
59 Air Temperature change (ΔGSAT) was introduced by adjusting HadCRUT4 ΔGMST to account
60 for incomplete coverage and discrepancy in measured air and ocean water temperature anomalies

61 (Rogelj et al., 2018; Cowtan et al., 2015). The Δ GSAT estimate of 0.97°C in 2006-2015 implied
62 lower remaining carbon budgets compared to preceding studies based on Δ GMST consistent
63 with AR5's 0.85°C through 2012 (Millar et al., 2017a, 2017b; Goodwin et al., 2018; Richardson
64 et al., 2018).

65
66 IPCC AR5 Box 2.2 discusses issues with linear trends for estimating Δ GMST: 1) poor
67 approximation of trend evolution over time; 2) poor fit of residuals unamenable to correction via
68 autoregressive or moving average models; 3) high sensitivity to selected period; and 4) divergent
69 or even contradictory sub-period estimates relative to that of a larger encompassing interval. The
70 latter two issues were particularly relevant in AR5 Section 2.4.3's discussion of the "observed
71 reduction in warming trend" over 1998-2012 compared to 1951-2012 (Rahmstorf et al., 2017;
72 Risbey et al., 2018). A smoothing spline non-linear trend fit was demonstrated to address these
73 factors, and later studies presented alternative estimators for continuous long-term Δ GMST
74 trends (Cahill et al., 2015; Peng-Fei et al., 2014; Mudelsee, 2019; Visser et al., 2018).

75
76 An issue of particular concern is that linear trends underestimate long-term Δ GMST compared to
77 other estimates. For example, IPCC AR5 Box 2.2 estimated HadCRUT4 1900-2012 trends of
78 $0.075 \pm 0.013^{\circ}\text{C decade}^{-1}$ and $0.081 \pm 0.010^{\circ}\text{C decade}^{-1}$ for linear OLS and smoothing spline
79 trends respectively. Generally, long-term linear fit Δ GMST is $0.05 - 0.10^{\circ}\text{C}$ below nonlinear
80 estimates (SR15 table 1.2; Visser et al., 2018) although the spread in Δ GMST estimates between
81 different datasets is commonly as wide as differences engendered by Δ GMST methodology.
82 Ultimately, IPCC AR5 Box 2.2 recommended linear trends over non-linear estimates, noting that
83 HadCRUT4' OLS-based long-term Δ GMST lay within the 5-95% uncertainty range of
84 smoothing spline. Nevertheless, as the IPCC enters the AR6 assessment, a new method that
85 supplements or supplants the traditional approaches could reduce known biases and address these
86 shortcomings.

87
88 This work proposes a local regression technique (LOESS, Cleveland et al., 1992; Cleveland,
89 1979) with a ± 20 year smoothing window for multi-decadal analysis. We also provide a
90 statistical error and show that the fit residuals follow the assumed autocorrelation structure. The
91 framework can be extended to give self-consistent Δ GMST estimates with uncertainty over as
92 little as 15 years, providing a potential alternative to linear fits over all intervals of interest.

93
94 However, here we focus on long-term Δ GMST and associated carbon budgets, and directly relate
95 our estimates to approaches discussed in AR5 and SR1.5. We compare against the IPCC
96 approaches of OLS (1880—latest year) and period mean differences (between 1850—1900 and
97 latest decade), plus a global warming index which SR1.5 used as the main example of "more
98 formal methods of quantifying externally driven warming" (Haustein et al., 2017). We also test
99 the performance of our LOESS estimates using output from the two model large ensembles that
100 begin in 1850. A final comparison is with the new CMIP6 model ensemble, and using a subset of
101 this ensemble we derive a modest conversion factor to update our observation-based Δ GMST to
102 Δ GSAT for carbon budget calculations.

103
104 The paper is structured as follows. Section 2.1 describes source data from observations (2.1.1),
105 CMIP6 models (2.1.2), two large model ensembles (2.1.3). Section 2.2 describes trend
106 estimation (2.2.1), evaluation of Δ GMST methods and performance (2.2.2), large model

107 ensemble evaluation (2.2.3) and Δ GSAT and carbon budget calculation (2.2.4). We present our
108 results in Section 3, covering long-term Δ GMST analysis (3.1), large model ensemble analysis
109 (3.2) and Δ GSAT and associated remaining carbon budgets (3.3). Finally we discuss our results
110 and issue recommendations in Section 4.

111

112 **2 Source Data and Methods**

113 **2.1 Source Data**

114 IPCC discussions of temperature change and carbon budgets include multiple sources and
115 approaches. We now remind the reader of our approach and justify each component. This
116 Section lists data sources, including temperature datasets and the forcing datasets required to
117 derive a global warming index referenced in SR1.5 as a potential alternative to Δ GMST for
118 tracking anthropogenic warming. Two large ensembles are included to allow performance tests
119 of each Δ GMST calculation method and CMIP6 data are added for updated model-observation
120 Δ GMST comparisons and to derive an adjustment from Δ GMST to Δ GSAT.

121 2.1.1 Global surface temperature datasets Typically, gridded monthly land surface air temperature
122 (LSAT) and sea surface temperature (SST) anomalies are generated then blended to produce
123 GMST. Table 1 summarizes five blended LSAT-SST series in widespread use. There is
124 considerable overlap in the underlying datasets. There are two SST data sets: HadSST3
125 (Kennedy et al., 2011) and NOAA's ERSSTv5 (Huang et al., 2017), and three LSAT datasets:
126 GHCNv4 (Menne et al., 2019), CRUTEM4 (Jones et al., 2010), and BerkeleyEarth (Rohde et al.,
127 2011). Even this understates the overlap; for example, both SST datasets rely primarily on the
128 comprehensive store of maritime observations from the International Comprehensive Ocean-
129 Atmosphere Data Set (ICOADS, Freeman et al., 2016), albeit processed, filtered and
130 supplemented in different ways.

131

132 **Table 1.** Five operational observational datasets.

Series	Land (LSAT)	Ocean (SST)	Interpolation	Averaging	Start year
HadCRUT4 (Morice et al., 2012)	CRUTEM4	HadSST3	None	Hemisphere average of gridboxes	1850
NOAA GlobalTemp v5 (Zhang et al., 2019)	GHCNv4	ERSSTv5	EOTs	Area weighted average	1880
NASA GISTEMP v4 (Lenssen et al., 2019)	GHCNv4	ERSSTv5	Distance weighting (to 1200 km)	80 zones x 100 sub-boxes	1880
Cowtan-Way v2 (Cowtan & Way, 2014a; Cowtan & Way, 2014b; Cowtan et al., 2015)	CRUTEM4 (kriged)	HadSST3 (kriged)	Kriging (Complete)	Area weighted average	1850
Berkeley Earth (Rohde et al., 2013)	Berkeley Earth	HadSST3 (reprocessed & kriged)	Kriging (to 1200 km)	Area weighted average	1850

133 Differences in spatial interpolation can affect calculated GMST. HadCRUT4 calculates area-
 134 weighted hemispheric means with no interpolation between its 5°×5° grid boxes. In contrast,
 135 NASA GISTEMP, Cowtan-Way and Berkeley Earth use extensive interpolation and, crucially,
 136 extrapolate LSAT over sea ice. Comparisons with temperature reanalyses, independent surface
 137 data and satellite retrievals show that this significantly reduces coverage bias arising from poor
 138 sampling of the fastest warming areas, especially the Arctic, since the mid-twentieth century
 139 (Dodd et al., 2015; Cowtan et al., 2018a; Susskind et al., 2019). Evidence is mixed for earlier
 140 periods where reduced coverage leads to larger interpolation uncertainty (Cowtan et al., 2018)
 141 and differences between underlying SST datasets are the largest source of discrepancies.
 142 GISTEMP and Berkeley Earth’s interpolated areal coverage is two to three times that of
 143 HadCRUT4 in the late 19th century, and is virtually complete since 1951 (See Figure S1,
 144 Supplementary Information). NOAA GlobalTemp’s interpolation results in coverage between
 145 that of HadCRUT4 and NASA GISTEMP, but largely misses very high latitudes and has no
 146 coverage over Arctic sea ice.

147 We use the published monthly anomaly series, except for Berkeley Earth where we use the area-
 148 weighted average of the gridded series, which diverges from the published series over 1850—
 149 1950 (Supplementary Information, Figure S2, S3). For series starting in 1850 anomalies are
 150 relative to 1850-1900 while NASA GISTEMP and NOAA GlobalTemp are baselined such that
 151 their 1880-1900 mean matches that of the three longer-running datasets. This allows NASA and
 152 NOAA Δ GMST estimates from 1850-1900 in a consistent manner, replacing the IPCC SR1.5

153 approaches based on scaling their 1880—2015 trends or matching to HadCRUT4 over 1880-
 154 1990. We also report the mean $\Delta GMST$ for all five datasets (OpAll group) and the subset of
 155 three datasets with near-global post-1950 coverage (Global_3 group). Group $\Delta GMST$ estimates
 156 are the mean of the individual estimates as in IPCC AR5.

157 We augment temperature data with summarized anthropogenic and natural radiative forcing data
 158 from Hausteine et al (2017). These are used to estimate anthropogenic and natural forced changes,
 159 $\Delta GMST_{F,anthro}$ and $\Delta GMST_{F,nat}$, using a two-box impulse-response model with parameters
 160 derived from a least-squares-fit between observed temperatures and the modelled response (Otto
 161 et al., 2015; Hausteine et al., 2017). These estimates are used to assess the characteristics of a
 162 particular LOESS window choice (section 2.2.1) and as an additional comparator to long-term
 163 $\Delta GMST$.

164 2.1.2 Model Large Ensembles

165 Conceptually, we first decompose $\Delta GMST$ as:

$$166 \quad \Delta GMST = \Delta GMST_F + \Delta GMST_{var} \quad (1)$$

167 where $\Delta GMST_{var}$ represents internal variability and $\Delta GMST_F$ the forced response. We adopt the
 168 IPCC SR1.5 argument that “[s]ince 2000, the estimated level of human-induced warming has
 169 been equal to the level of observed warming with a *likely* range of $\pm 20\%$ ”. From this it follows
 170 that a reliable estimate of $\Delta GMST_F$ through 2019 would be an appropriate estimate of human-
 171 induced warming, $\Delta GMST_{F,anthro}$, with relevance for temperature targets and carbon budgets.
 172 With just one realization of real-world internal variability we cannot perform this decomposition,
 173 but a large ensemble mean should approach that model’s $\Delta GMST_F$. We test whether our derived
 174 $\Delta GMST_{LOESS}$ approximates $\Delta GMST_F$, and consider the decomposition in an individual run to be:

$$175 \quad \Delta GMST = \Delta GMST_{LOESS} + \Delta GMST_{resid} \quad (2)$$

176 With a ± 20 -year window this effectively decomposes between short- and long-term $\Delta GMST$. If
 177 periods are selected to minimize volcanism (which induces short-term $\Delta GMST_F$), and the
 178 magnitude of $\Delta GMST_{var}$ is small at 40-year timescales, then resultant $\Delta GMST_{LOESS} \approx$
 179 $\Delta GMST_{F,anthro}$.

180 These tests use output from the large ensembles whose simulations begin in 1850: the Max
 181 Planck Institute for Meteorology Grand Ensemble (MPI-GE, N=100, Maher et al., 2019) and
 182 Commonwealth Scientific and Industrial Research Organisation Mk3.6.0 (CSIRO Mk3.6.0,
 183 N=30, Rotstayn et al., 2012; Jeffrey et al. 2013), taking their GSAT over historical-RCP8.5
 184 simulations for 1850—2019 and baselining each to 1850—1900. We exclude five other large
 185 ensembles that start after 1850 (Deser et al, 2020), and our approach is conceptually similar to
 186 that in Dessler et al. (2018)’s estimation of how internal variability affects derived climate
 187 sensitivity in MPI-GE. The use of GSAT simplifies the calculations and since the year-to-year
 188 variability in GSAT-GMST difference is of order 0.01 °C in CMIP5 models (e.g. Figure 2 of
 189 Cowtan et al. 2015), we expect little effect of blending or masking on this particular analysis.

190 2.1.3 Climate Model Intercomparison Project, phase 6 (CMIP6) output

191 We include historical simulations over 1850-2014 from CMIP6 models which have the required
 192 fields for blending surface air temperatures (SAT) over land or sea ice and SST over ocean
 193 (Eyring et al, 2016), permitting “apples-to-apples” comparisons with land-ocean observational
 194 datasets. These include near-surface air temperature (“tas”), sea surface temperature (“tos”) and
 195 sea ice concentration (“sciconc” or “sciconca”, N=24 simulations listed in Table S1).

196 Following Cowtan et al (2015) and Richardson et al (2018), each simulation is processed to
 197 produce two series: 1) global SAT and 2) global blended SAT-SST. At each grid cell i, j , the
 198 blended monthly temperature $T_{\text{blend},i,j}$ is:

$$199 \quad T_{\text{blend},i,j} = w_{\text{SAT},i,j} T_{\text{SAT},i,j} + (1 - w_{\text{SAT},i,j}) T_{\text{SST},i,j} \quad (3)$$

200 where $w_{\text{SAT},i,j}$ is the land plus sea ice grid cell fraction, and $T_{\text{SAT},i,j}$ and $T_{\text{SST},i,j}$ are the local
 201 anomalies relative to 1850-1900. For global SAT $w_{\text{SAT},i,j} = 1$ everywhere, and for the blended
 202 series $w_{\text{SAT},i,j} = 1$ in ocean cells for a calendar month if any those months during 1961-2014 has
 203 siconc > 1%. This is similar to the Cowtan-Way blending algorithm and the “xaf” simulations in
 204 Cowtan et al. (2015).

205 2.2 Methods

206 Next we describe our approach to obtain ΔGMST , our uncertainty estimation, and the remaining
 207 carbon budget calculation. Section 2.2.1 explains the trend fits and errors, Section 2.2.2 explains
 208 the ΔGMST calculations, observational error and methods by which the fit quality are judged
 209 using observational data. Section 2.2.3 discusses the large ensemble methodology, Section 2.2.4
 210 the CMIP6 comparison and carbon budget calculation.

211 2.2.1 Trend calculations and their statistical uncertainty

212 For a series of n temperature observations x_i at time t_i , a linear trend is:

$$213 \quad x_i = a + bt_i + e_i, \quad i = 1, \dots, n \quad (4)$$

214 where a and b are intercept and slope parameters to be fitted and e_i are residual errors. The slope
 215 estimate \hat{b} is used to obtain ΔGMST as $\hat{b}(t_n - t_i)$, with the uncertainty of \hat{b} (and thus ΔGMST)
 216 determined as explained below.

217 Our multidecadal LOESS point-to-point (LOESS_{md}) ΔGMST is based on the LOESS fit from
 218 1880—2019; for any starting point, ΔGMST to 2019 is the LOESS_{md} fit evaluated in 2019 minus
 219 the start value. We also introduce “baseline” LOESS (LOESS_{bsln}) as our main ΔGMST estimate.
 220 LOESS_{bsln} is simply the same fit evaluated at the end year, yielding an estimate relative to
 221 1850—1900 baseline, rather than to a given start year such as 1880.

222 Our LOESS_{md} uses a fixed span α_{md} of ± 20 years, tricube weighting (the default) and a degree 1
 223 smoothing parameter (i.e. locally weighted linear trend, which yields more stable end points).
 224 Tests with the Cowtan-Way series show that α of ± 10 years captures internal decadal variability
 225 and has marked sensitivity to volcanic episodes early in the record and to a lesser extent over

226 1980-2019 (Figure S4). On the other hand, α of ± 20 or ± 30 years smooth out short-term
 227 variability and show similar warming from 1850-1900 to present: 1.12°C (± 20 years) or 1.11°C
 228 (± 30 years). Analysis of first differences for each LOESS window (Figures S6, S7) show large
 229 variance with α of ± 5 years, which stabilises with α of ± 20 , ± 25 or ± 30 years. Large ensemble
 230 tests support this choice: α_{md} substantially smaller than ± 20 years increases ΔGMST_F
 231 discrepancy, while substantially longer than ± 20 years introduces a low bias in 1850—2019
 232 ΔGMST (Figures S6, S7). We therefore choose $\alpha_{md} = \pm 20$ years to evaluate trends of length ≥ 30
 233 years; $\text{LOESS}_{\text{pent}}$ ($\alpha = \pm 5$ years) is reserved for future extension of our framework to cover very
 234 short-term trends of ≤ 15 years (see Figure S4, panel d).

235 Default methods assume statistically independent noise, necessitating an uncertainty correction if
 236 the fit residuals are autocorrelated. Santer et al (2000) presented a procedure for assessing an
 237 effective sample size (and associated reduction in degrees of freedom) from the general formula

$$238 \quad n_e = \frac{n_t}{(1 + 2 \sum_{j=1}^{n-1} \rho_j)} \quad (5)$$

239 where ρ_j is the autocorrelation function of a noise model estimated from the fit residuals. If the
 240 noise follows an autoregressive(1) (AR(1)) process, then with $\rho_j = \phi^j$
 241

$$242 \quad 1 + 2 \sum_{j=1}^{n-1} \rho_j \approx 1 + \frac{2\phi}{(1-\phi)} = \frac{(1+\phi)}{(1-\phi)} \quad (6)$$

243 where ϕ is estimated from the lag-one autocorrelation coefficient (Mitchell et al, 1966).
 244 However, Foster and Rahmstorf (2011) demonstrated that 1979-2010 GMST trend residuals
 245 were more consistent with an autoregressive moving average, ARMA(1, 1) model in the form

$$246 \quad \rho_1 = \frac{(\phi + \theta)(1 + \phi\theta)}{1 + 2\phi\theta + \theta^2} \quad (7)$$

$$\rho_j = \rho_1 \phi^{j-1} \quad j \geq 2$$

247 Substituting (6) into (5) yields

$$248 \quad 1 + 2 \sum_{j=1}^{n-1} \rho_j \approx 1 + \frac{2\rho_1}{(1-\phi)} \quad (8)$$

249 Foster and Rahmstorf used the Yule-Walker “method of moments” with $\hat{\phi} = \hat{\rho}_1 / \hat{\rho}_2$. Hausfather
 250 et al. (2017) instead used Maximum Likelihood Estimation (MLE) to obtain $\hat{\phi}$ and $\hat{\theta}$ and then $\hat{\rho}_1$
 251 via Eq. (6). Monte Carlo simulations show that MLE gives a more robust and efficient estimator
 252 $\hat{\phi}$, suitable for series as short as 8 years (see Figure S8). Hausfather et al. also introduced a bias
 253 correction to account for underestimated autocorrelation in shorter series, derived from AR(1) in
 254 Tjøstheim and Paulsen (1996) and extended to account for the positive difference between $\hat{\phi}$ and
 255 $\hat{\rho}_1$.

$$\begin{aligned} \hat{\phi}_{BC} &= \hat{\phi} + \left(1 + 4(2\hat{\phi} - \rho_1)\right) / n_t \\ \rho_{1BC} &= \rho_1 + \left(1 + 4(2\hat{\phi} - \rho_1)\right) / n_t \end{aligned} \quad (9)$$

257 Although this bias correction is most pertinent for very short series, Monte Carlo simulations
 258 have demonstrated its relevance for highly autocorrelated series up to 720 months in length. We
 259 selected this bias correction after comparison with alternatives (e.g. Nychka et al., 2000; see
 260 Figure S9).

261 Substituting the bias corrected parameters and simplifying the correction term as in (5) yields the
 262 final effective length correction.

$$n_e = \frac{n_t}{1 + 2 \sum_{j=1}^{n-1} \rho_j} \approx \frac{n_t}{1 + 2\rho_{1BC} / (1 - \hat{\phi})} \quad (10)$$

264 We estimate corrections from the residuals of both LOESS and OLS. To apply this correction,
 265 we define nominal degrees of freedom $\nu = n_t - p$ and effective degrees of freedom $\nu_e = n_e - p$,
 266 where p is the number of actual or equivalent parameters of the trend fitting methodology.

267 In the linear case, the correction is applied directly to s_b , the standard error of b in (1), with $p = 2$.

$$s'_b = s_b \frac{\nu}{\nu_e} = s_b \frac{n_t - 2}{n_e - 2} \quad (11)$$

269 For non-parametric trend estimation like LOESS, Monte Carlo simulations can establish
 270 uncertainties, as in Visser et al (2016) for smoothing spline trends. Here we propose a plausible
 271 heuristic method. First the above correction is applied to s_e , the standard errors of the residual fit,
 272 with p set to the equivalent number of parameters of the LOESS trend, derived from the trace of
 273 the LOESS projection matrix (Cleveland and Grosse, 1991); generally $p \approx 2/\alpha + 0.5$ for GMST
 274 datasets. For an equally spaced time series, s_e is maximum at the start and end of the LOESS fit.
 275 If errors at these two points are independent, the corrected standard error $s'_{\Delta T_n}$ for ΔGMST_n
 276 becomes

$$s'_{\Delta T_n} = \sqrt{2} \max(s'_e) = \sqrt{2} \max(s_e) \frac{n_t - p}{n_e - p} \quad (12)$$

278 For both OLS and LOESS_{md} we evaluate the sample autocorrelation function (ACF) of the fit
 279 residuals as well as the ACFs of the ARMA(1, 1) and AR(1) noise models fit to those residuals.
 280 Finally, for LOESS_{bsln} we assume that the mean error during 1850—1900 is very small relative
 281 to the end point error and so its error is taken to be:

$$s'_{\Delta T_n} = \max(s'_e) = \max(s_e) \frac{n_t - p}{n_e - p} \quad (13)$$

283 Monte Carlo simulations of LOESS fits plus ARMA(1, 1) noise produce a probability
 284 distribution function nearly identical to that engendered in Cowtan-Way by (11) over 1880-2019
 285 and by (12) from 1850—1900 to 2019 (Figures S10 and S11).

286 2.2.2 Estimates of observational Δ GMST, error components and performance tests

287 The main analysis focuses on long-term Δ GMST (results for other IPCC AR5 periods are in the
 288 Supplementary Information Table S2). In addition to OLS and LOESS_{md} Δ GMST over 1880-
 289 2019, and LOESS_{bsln} from 1850-1900 to 2019, we also calculate period difference Δ GMST
 290 estimates by subtracting mean GMST over 1850—1900 from the most recent decade, 2010-
 291 2019. The above are also compared to GMST-derived estimates of anthropogenic warming
 292 (Haustein et al., 2017; section 2.1.2) and to a CMIP6 ensemble (Section 2.2.4). Global_3 and
 293 OpAll group Δ GMST are the mean of individual dataset Δ GMST.

294 Following standard IPCC practice, we report the 5-95% statistical uncertainty range for LOESS
 295 and OLS Δ GMST estimates, as outlined in Section 2.2.1. Group uncertainties are reported
 296 conservatively and go from the smallest 5% to the largest 95% reported for any of their
 297 constituent datasets. We also report observational parametric uncertainty as the 5—95 % range
 298 of Δ GMST values derived from each of the 100-member HadCRUT4 and Cowtan-Way
 299 ensembles. These ensembles use a Monte-Carlo method to assess the fully correlated errors
 300 engendered by parametric uncertainty related to bias adjustments to individual temperature
 301 readings (Kennedy et al., 2011).

302 Figure S13 depicts these estimates and derived autocorrelation functions (ACF) for the Cowtan-
 303 Way monthly series with ARMA(1, 1) correction and for Cowtan-Way annual series with AR(1)
 304 correction (similar to IPCC AR5).

305 Finally we assess LOESS_{bsln} Δ GMST against period mean differences for the Global_3 group by
 306 evaluating at the mid-point of the corresponding end decade; for example, LOESS_{bsln} at the end
 307 of 2014 is comparable to the 1850-1900 to 2010-2019 period Δ GMST. IPCC SR1.5 explicitly
 308 considered their 1850—1900 to 2006-2015 Δ GMST estimate to be a proxy of the eventual 1996-
 309 2025 mean. We therefore compare the Δ GMST estimates for every year from 1995 against
 310 centered 20-year and 30-year means. We also compare to “extended” running 30-year periods,
 311 generated by assuming a continuation of the 1990-2019 linear trend through 2029. We argue that
 312 a smaller bias and root mean square error (RMSE) relative to the 20- and 30-year means
 313 represents better performance according to the IPCC’s own criterion.

314 2.2.3 Large Ensemble Analysis for Method Validation and Uncertainty Calculation

315 LOESS_{bsln} is fit to the 1850—2019 annual output for each simulation, then the Δ GMST through
 316 2019 is evaluated from all start years 1850—1980. Separate linear OLS fits ending in 2019 are
 317 also obtained for those start years. We also evaluate LOESS_{bsln} at the end of 2014 and compare
 318 with the 1850—1900 to 2010—2019 period Δ GMST. Finally, LOESS_{md} is calculated over
 319 1880—2019 for each simulation. The distribution of ensemble member Δ GMST- Δ GMST_F
 320 provides an estimate of the bias and uncertainties for each estimator and each period, as argued
 321 in Section 3.2. If Δ GMST_{LOESS} \approx \DeltaGMST_F then the LOESS residuals will be dominated by}

322 internal variability and our statistical uncertainty is related to error due to internal variability (we
 323 confirmed that the model residuals generally follow our assumed ARMA(1,1), Figure S14). The
 324 LOESS decomposition filters in time: $\Delta GMST_F$ excursions shorter than our window will inflate
 325 statistical error, while multidecadal $\Delta GMST_{var}$ changes will be included in $\Delta GMST_{LOESS}$ and
 326 result in too small errors. We compare each run’s statistical uncertainties with the ensemble 17—
 327 83 % and 5—95 % ranges to check for evidence that the observation-derived statistical
 328 uncertainties could represent internal variability in the $\Delta GMST$ used for carbon budget
 329 calculations (see Section 2.2.4).

330 2.2.4 CMIP6 comparisons, GSAT adjustment and remaining carbon budget

331 IPCC SR15 reported remaining carbon budgets accounting for warming to date, but did not
 332 directly use the reported $\Delta GMST$ 5—95 % observational uncertainty from individual datasets.
 333 Instead AR5 5—95 % observational uncertainty through 1986-2005 was combined with
 334 additional uncertainties to produce a “likely” 17—83 % $\Delta GMST$ total uncertainty and $\Delta GMST$
 335 was then converted to $\Delta GSAT$ using a CMIP5-derived scaling. This Section describes the
 336 comparison with CMIP6 $\Delta GMST$ and conversion of observed $\Delta GMST$ to $\Delta GSAT$, and then
 337 details the carbon budget calculation, which largely follows the IPCC SR1.5 recipe .

338 LOESS series are generated for each CMIP6 air-only (GSAT) and blended (GMST) series, with
 339 the blended series being comparable to GMST observations. We consider the full ensemble and
 340 also a sub ensemble of “likely ECS” models, excluding those with effective climate sensitivity
 341 (ECS) outside the CMIP5 1.9-4.5°C 90% ensemble range (Flato et al., 2013; Forster et al.,
 342 2019).

343 For each ensemble member’s $LOESS_{bsln}$ changes we derive a “blending” factor $A_{blend} = \Delta GSAT /$
 344 $\Delta GMST$, and the ensemble A_{blend} is used to scale observed $\Delta GMST$ to obtain historical $\Delta GSAT$
 345 for calculating the remaining carbon budget. The carbon budget calculation follows the
 346 framework established in IPCC SR1.5 (Rogelj et al., 2017), elaborated by Rogelj et al (2019) and
 347 implemented by Nauel et al (2019). We simplify the Rogelj et al (2019) remaining carbon budget
 348 equation to:

$$349 \quad B_{lim} = \left(\Delta GSAT_{lim} - \Delta GSAT_{hist} - \Delta GSAT_{nonCO_2, fut} \right) / TCRE - E_{Esfb} \quad (13)$$

350 where B_{lim} is the remaining carbon budget associated with a temperature limit $\Delta GSAT_{lim}$ (1.5 or
 351 2°C), with $\Delta GSAT_{hist}$ the historical human-induced warming to date and $\Delta GSAT_{nonCO_2, fut}$ the
 352 expected future warming from non-CO₂ anthropogenic forcing. TCRE is the transient climate
 353 response to cumulative CO₂ emissions, while E_{Esfb} is an adjustment for Earth system feedbacks
 354 from permafrost thaw and warming wetlands. From the finding that observed and “human-
 355 induced” warming to date are approximately equivalent (Allen et al., 2018; Haustein et al.,
 356 2017), SR15 assessed $\Delta GSAT_{hist}$ as 0.97°C in 2006-2015 relative to 1850-1900, based on the
 357 HadCRUT4 average for that decade (0.84°C) adjusted by the ratio between the equivalent
 358 CMIP5 blended-masked estimate (0.86°C) and CMIP 5 GSAT (0.99°C).

359 Here we select the Global_3 GMST group and so do not need to rely on a model correction for
 360 the bias introduced by HadCRUT4’s incomplete and changing geographic coverage, which is
 361 substantially larger than A_{blend} . Our estimate for $\Delta GSAT_{hist}$ is:

$$362 \quad \Delta GSAT_{hist} = A_{blend} \Delta GMST_{Global_3} \quad (14)$$

363 where A_{blend} is the median value from CMIP6 ensemble members and $\Delta GMST_{Global_3}$ is the
 364 LOESS_{bsln} $\Delta GMST$ of the Global_3 group (based on the mean of LOESS_{bsln} applied to each of
 365 the three series). It should be noted this is a very conservative adjustment, as it may not fully
 366 account for coverage bias in the early part of the instrumental record, and ignores the “ice edge
 367 effect” cooling bias introduced by the variable sea ice mask in NASA GISTEMP and Berkeley
 368 Earth (Cowtan et al., 2015; Richardson et al., 2018).

369 SR1.5’s likely total uncertainty in $\Delta GMST$ and $\Delta GSAT_{hist}$ was $\pm 0.12^\circ\text{C}$. Here we derive likely
 370 $\Delta GSAT$ using Gaussian approximations to the observational, dataset spread and statistical fit
 371 uncertainties in the following steps (tests and details in Supplementary Table S3):

- 372 1. The Cowtan-Way ensemble spread is our best estimate of observational parametric
 373 $\Delta GMST$ uncertainty, so for each dataset its standard deviation is combined in quadrature
 374 separately with (i) the dataset-specific statistical 1σ uncertainty and (ii) the CSIRO
 375 Mk3.6.0 large ensemble standard deviation.
- 376 2. For $\Delta GSAT$, the CMIP6 A_{blend} ensemble standard deviation is taken as the uncertainty
 377 value, and combined in quadrature with the results of 1.
- 378 3. We estimate a 17—83 % range by calculating those percentiles for each dataset following
 379 a Gaussian assumption, i.e. $\pm 0.954\sigma$ from the mean, and then selecting the lowest 17 %
 380 and higher 83 % value from across the datasets.

381 There is no universally accepted method of accounting for dataset spread. We adopt step 3 as a
 382 conservative approach, however, by reporting the separate dataset uncertainties as described in
 383 Section 2.2.2 other groups can replicate or develop alternative uncertainty estimates.

384 We take Rogelj et al. (2019)’s, T_{nonCO_2} of 0.1°C (0.2°C) for T_{lim} of 1.5°C (2°C), and E_{Esfb} of 100
 385 Gt CO_2 through 2100. TCRE percentiles are based on AR5’s likely range of $0.2\text{--}0.7^\circ\text{C}$ per 1,000
 386 Gt CO_2 (Collins et al., 2013), as in Nauels et al (2019). SR1.5 included alternative carbon
 387 budgets using a lower T_{hist} from the average of the blended GMST datasets with no GSAT
 388 adjustment. Our alternative uses the Global_3 average without the GSAT adjustment. To
 389 contextualize the remaining budget against cumulative emissions to date we include data and
 390 uncertainties from the 2019 Global Carbon Budget (Friedlingstein et al., 2019).

391

392 **3 Results**393 3.1 Long term Δ GMST analysis

394 Figure 1 compares LOESS_{md} and OLS Δ GMST from 1880—2019 with associated 5—95%
395 uncertainties (Fig. 1a). Figure 1b shows that the LOESS fit residuals follow our assumed
396 ARMA(1, 1), which is necessary to justify our error correction and is not true for OLS (Figure
397 1c). Our full set of observational Δ GMST estimates are given in Table 2.

398 OLS Δ GMST is always lower than LOESS, with some even lying outside the LOESS
399 uncertainty range or nearly so (Cowtan-Way, Berkeley Earth). Datasets are similarly ranked for
400 both OLS and LOESS_{md} over 1880-2019, from HadCRUT4 (0.96, 0.99) to Berkeley Earth (1.05,
401 1.14). The Global_3 series exhibit a greater relative difference than the non-global series; the
402 Berkeley Earth and HadCRUT4 LOESS_{md} difference is 0.21°C, but only 0.13°C for OLS. Thus
403 OLS not only renders lower Δ GMST, but also de-emphasizes the differences between the
404 datasets.

405 We identify two factors that appear to contribute to the increased long-term LOESS_{md} Δ GMST
406 relative to OLS: improved recent coverage (Global_3 being higher than OpAll), and those using
407 HadSST relative to ERSSTv5. Improved coverage tends to increase recent trends, while the SST
408 datasets differ most strongly before and during WWII.

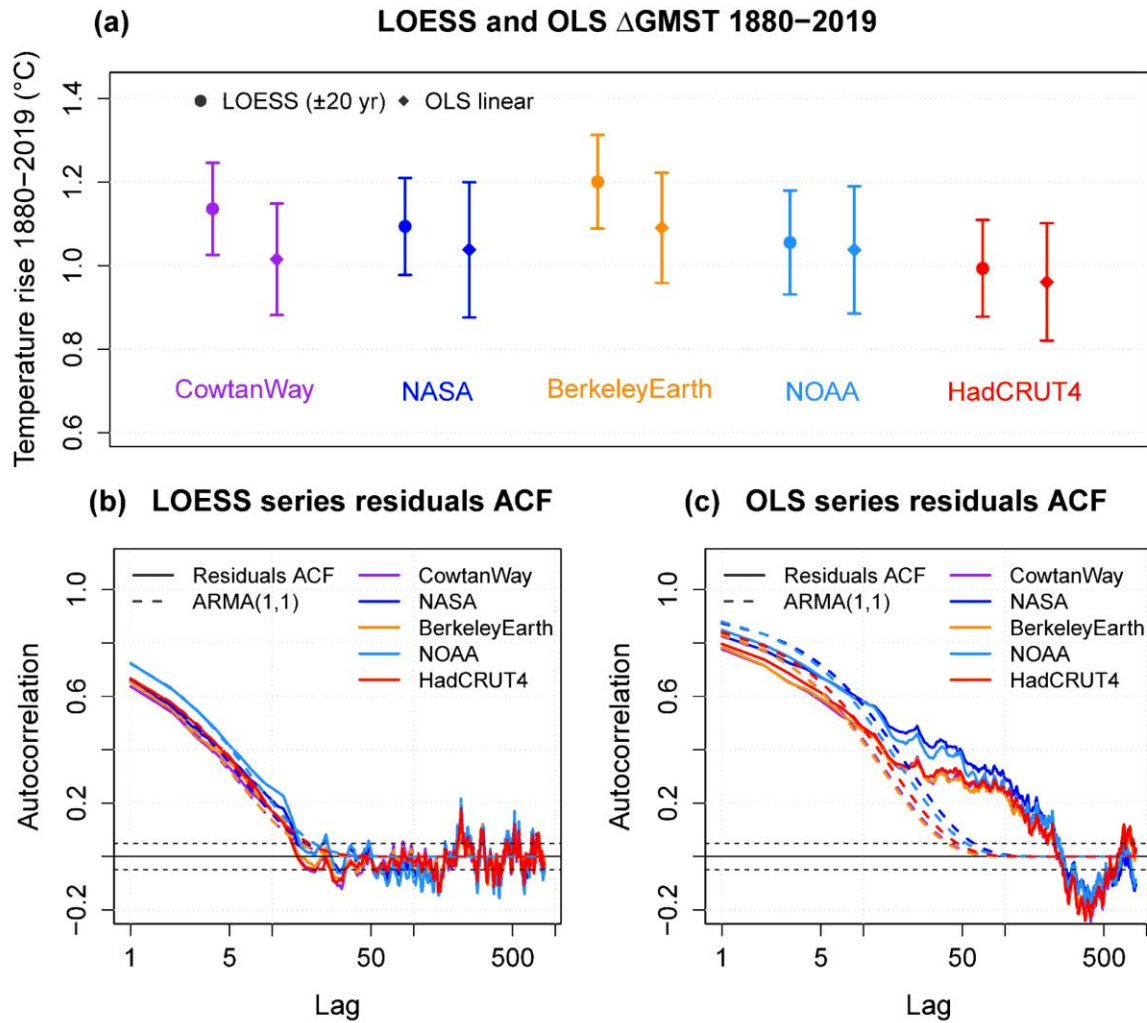
409

410

411

412

413



414
 415 **Figure 1: GMST series and 1880-2019 warming estimates.** (a) LOESS (span ± 20 years) and OLS trends with
 416 5-95% statistical fit uncertainty are shown for Cowtan and Way (purple), NASA GISTEMP (blue), Berkeley Earth
 417 (orange), NOAA GlobalTemp (light blue) and HadCRUT4 (red) over 1880-2019. (b) The autocorrelation function
 418 (ACF) of the LOESS fit residuals are shown for each series (solid lines), along with the ACF of the estimated
 419 ARMA(1, 1) model used to correct for autocorrelation. (c) As in (b) except for OLS linear trend..

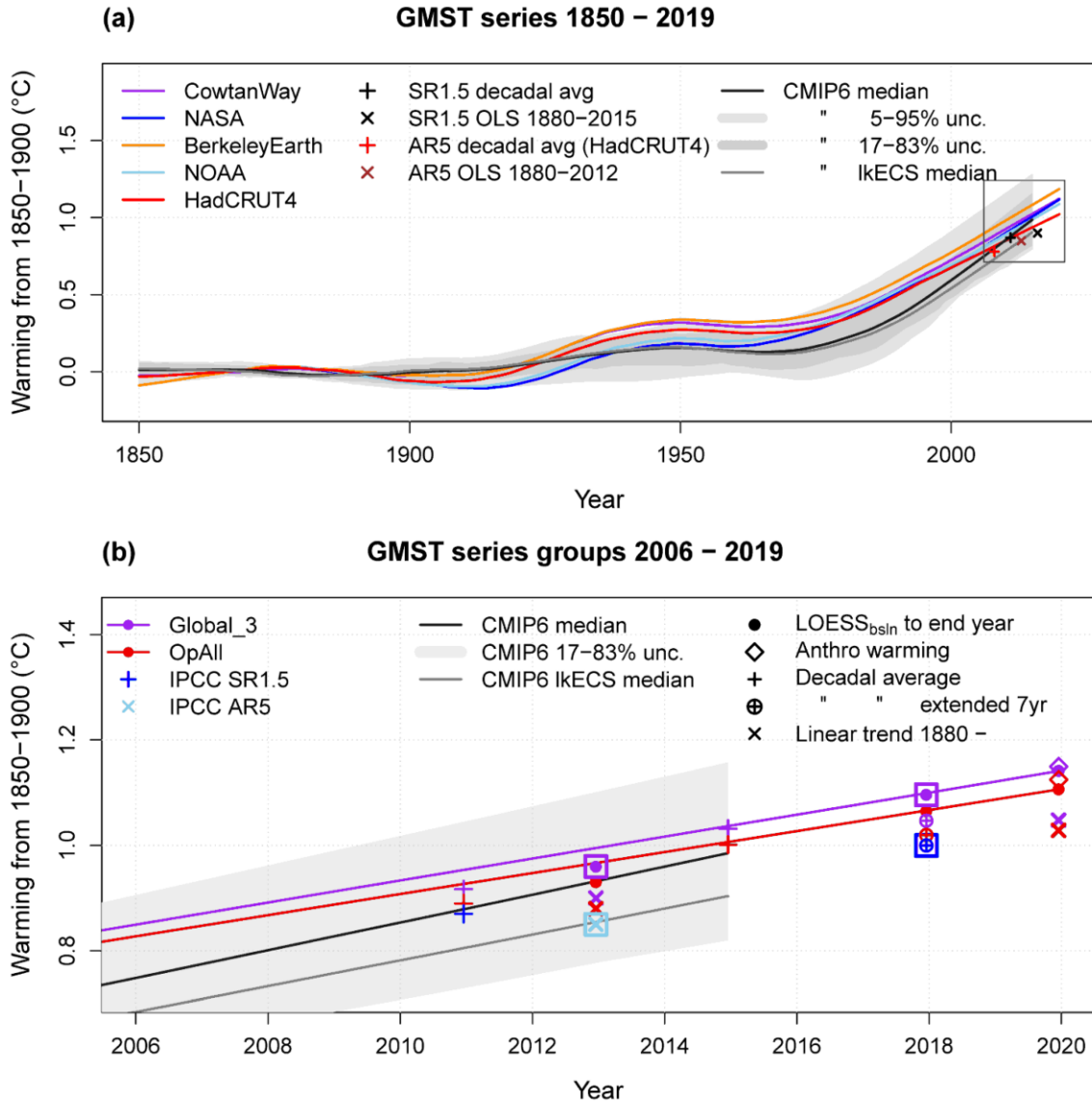
420
 421
 422
 423

424 **Table 2: Observed increase in GMST (°C) in datasets and dataset groupings.** Numbers in square
 425 brackets correspond to 5–95% statistical fit uncertainty ranges, accounting for autocorrelation in fit
 426 residuals. Round brackets denote observational parametric uncertainty where available (HadCRUT4,
 427 Cowtan & Way). NOAA and NASA are each aligned to match 1880-1900 mean of the other three
 428 datasets. Best estimates from three full global series are denoted by *. Group mean estimates (in bold) are
 429 given with uncertainties encompassing the spread from lowest 5% to highest 95%. For the Global_3
 430 group, the observational uncertainty is from Cowtan & Way, expanded by the spread of the three central
 431 estimates.
 432
 433
 434

<i>Period:</i> <i>Series:</i>	1850-1900 to 2019	1850-1900 to 2010-2019	1880 - 2019	
	LOESS _{bsln}	Latest decade	LOESS _{md}	Linear
HadCRUT4	1.02 [0.94 - 1.10] (0.97 – 1.07)	0.93 (0.88 - 0.98)	0.99 [0.88 - 1.11] (0.94 – 1.04)	0.96 [0.82 - 1.10] (0.92 – 1.03)
NOAA GlobalTemp	1.09 [1.00 - 1.18]	0.99	1.06 [0.93 - 1.18]	1.04 [0.89 - 1.19]
NASA GISTEMP	1.12 [1.03 - 1.20]	1.01	1.09 [0.98 - 1.21]	1.04 [0.88 - 1.20]
Cowtan & Way	1.12 [1.04 - 1.20] (1.05 – 1.19)	1.01 (0.95 - 1.09)	1.14 [1.03 - 1.25] (1.08 – 1.21)	1.02 [0.88 - 1.15] (0.94 – 1.09)
Berkeley Earth	1.19 [1.11 - 1.26]	1.08	1.20 [1.09 - 1.31]	1.09 [0.96 - 1.22]
All Operational	1.11 [0.94 - 1.26]	1.00	1.10 [0.88 - 1.31]	1.03 [0.82 - 1.22]
Full Global (3 series) *	1.14 * [1.04 – 1.26] (1.05 – 1.26)	1.03	1.14 [0.98 - 1.31]	1.05 [0.88 - 1.22]

435 For LOESS_{bsln} to 2019, there are minor differences in assessed values but no changes in dataset
 436 rankings versus LOESS_{md} 1880—2019. LOESS_{bsln} is generally ~0.1 °C higher than 1850-1900 to
 437 2010-2019 ΔGMST, reflecting the five-year offset and ~0.2 °C/decade recent warming (2010-
 438 2019 is centered at the end of 2014). At 1.14°C, Global_3 LOESS_{bsln} ΔGMST to 2019 is 0.03°C
 439 higher than OpAll average, reflecting a 0.09°C difference with the mean of the two reduced

440 coverage series from HadCRUT4 and NOAA GlobalTemp. The 1880—2019 LOESS_{md}
 441 discrepancy is even wider: 0.09°C for NOAA and 0.15°C for HadCRUT4. LOESS_{bsln} statistical
 442 fit uncertainties are smaller than LOESS_{md} or OLS, reflecting the smaller uncertainty of
 443 departure from the 1850—1900 mean rather than a single point (as noted in Section 2.2.2).



444
 445 **Figure 2: GMST series and group surface warming estimates.** (a) Monthly series and multi-decadal LOESS_{bsln}
 446 Δ GMST (span \pm 20 years) are shown for HadCRUT4 (red), NOAA GlobalTemp (light blue), NASA GISTEMP
 447 (blue), Cowtan and Way (purple) and Berkeley Earth (orange), together with OLS and period estimates from IPCC
 448 AR5 and SR15. NOAA GlobalTemp and NASA GISTEMP have been matched to the longer datasets over the
 449 overlapping 1880-1900 period. Also shown are 21 CMIP6 SAT-SST model runs, blended following Cowtan et al
 450 (2015) and Richardson et al (2018). (b) LOESS_{bsln} (solid line with filled circle) is shown for two GMST groupings:
 451 Global_3 (purple) and OpAll (dark red). Also shown are selected additional warming estimates: anthropogenic
 452 following Hausteine et al (2017) (diamonds), decadal average (crosses) and OLS linear trend from 1880 (x-crosses).
 453 Recent IPCC Δ GMST estimates are highlighted by large squares: AR5 OLS to 2012 (light blue) and SR1.5 2006-
 454 2015 mean extended to 2017 (blue), together with corresponding Global_3 LOESS_{bsln} Δ GMST (purple).

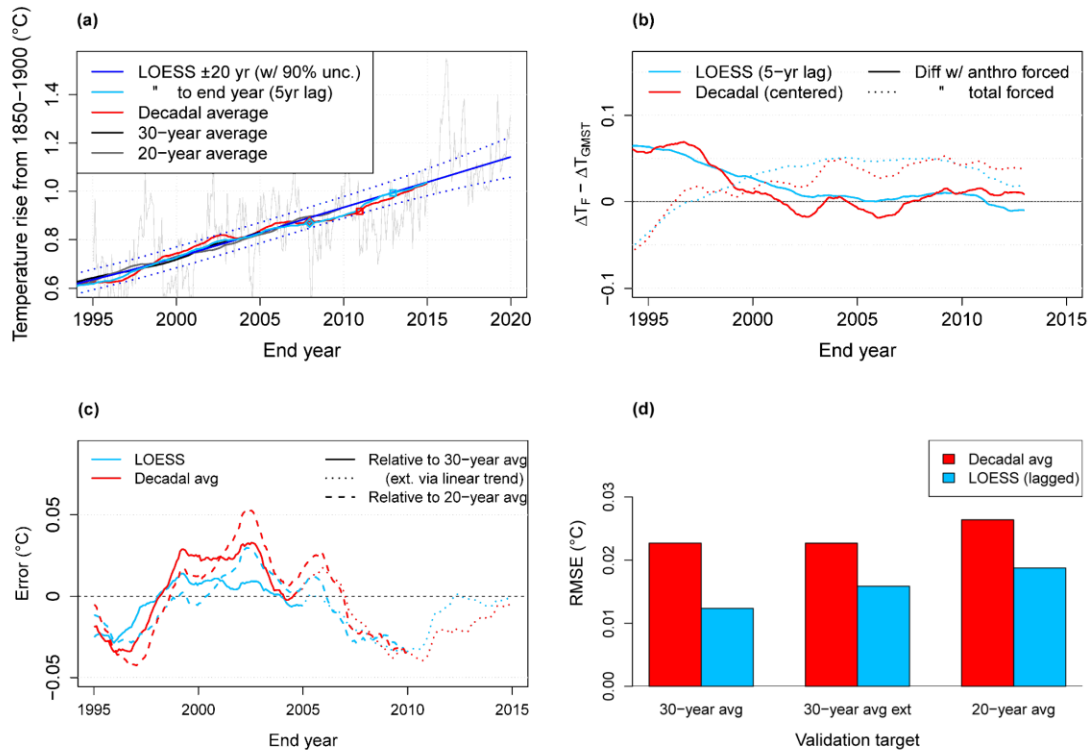
455 The observation-based and CMIP6 blended ensemble LOESS_{bsln} (Figure 2a) show broadly
456 similar changes: a rise to 1950, a 1950—1975 flattening, and strong post-1975 warming. The
457 observations show stronger 1920—1950 warming, especially in the three HadSST-based series,
458 and weaker post-1975 warming.

459 Separate tests showed that derived Δ GMST was similar when restricting CMIP6 spatial coverage
460 to that of Berkeley Earth, so we take the CMIP6 blended ensemble as directly comparable to the
461 Global_3 series (Figure S14). The Global_3 rise of 1.14°C is above the median CMIP6 estimate
462 extended linearly to 2019, 1.04°C [0.88 – 1.44]. However, the Global_3 incremental trend of
463 0.20°C/decade is lower than CMIP6’s 0.26°C/decade [0.18 – 0.38] or the likely ECS sub-
464 ensemble’s 0.25°C/decade [0.18 – 0.29].

465 In general, the observations are at or above recent IPCC long-term Δ GMST estimates. Figure
466 2(b) affords a closer view of recent Δ GMST estimates, including group LOESS_{bsln} calculated to
467 2012 and 2017 for direct comparison to IPCC AR5 and SR1.5. As previously stated, AR5’s main
468 estimate of 0.85°C was from linear OLS on the datasets available then. Since the mean 1880—
469 2012 OLS trend for OpAll is 0.89°C and LOESS_{bsln} is 0.93°C, Δ GMST methodology accounts
470 for half of the discrepancy between AR5’s 1880—2012 estimate and ours. The 2012 gap is even
471 wider for the Global_3 group; OLS to 2012 is 0.90°C and LOESS_{bsln} is 0.96°C; that gap
472 continues to grow, reaching 0.09°C in 2019.

473 The SR1.5 2006-2015 mean Δ GMST of 0.87°C was extended to 2017 to provide an up-to-date
474 estimate of 1.0°C (Section 1.2.1.3 in Allen et al., 2018). The same adjustment applied to the
475 updated series shows a 0.03°C gap with LOESS_{bsln}. This discrepancy may be related to internal
476 variability suppressing early 2000s warming; taking 2008-2017 or 2010-2019 removes the
477 LOESS-period discrepancy. Both LOESS_{bsln} and period estimates are in good agreement with the
478 slightly higher Haustein human-induced warming.

479 Figure 3 compares Global_3 LOESS_{bsln} and period Δ GMST in more detail. Since IPCC SR1.5
480 explicitly considered the 2006-2015 mean as a proxy for the 1996-2025 average (relative to
481 1850-1900), we consider the centered 20-year average and a 30-year “extended” average
482 assuming the current linear 30-year trend continues over the next 15 years. Figure 3a shows that
483 LOESS_{bsln} hews closer to the eventual average than the decade mean and confirms that 2006-
484 2015 was affected by an early 2000s slowdown. LOESS_{bsln} has more stability relative to
485 anthropogenic warming estimates (Figure 3b) and has lower RMSE relative to the longer period
486 averages since the late 1990s (Figure 3c, 3d).



487
 488 **Figure 3: ΔGMST estimation method validation based on average of 3 global series. (a) $\text{LOESS}_{\text{bsln}}$ to 2019**
 489 **(blue) is shown with 5-year lagged LOESS (light blue), decadal average (red), 20-year average (light gray)**
 490 **and 30-year average (dark gray). LOESS (light blue) versus decadal (red) differences are shown with (b) forced**
 491 **warming estimates following Haustein et al. (2017) and (c) validation targets (30-year average, 30-year average**
 492 **extended with linear trend and 20-year average). (d) RMSE is calculated from errors shown in (c).**

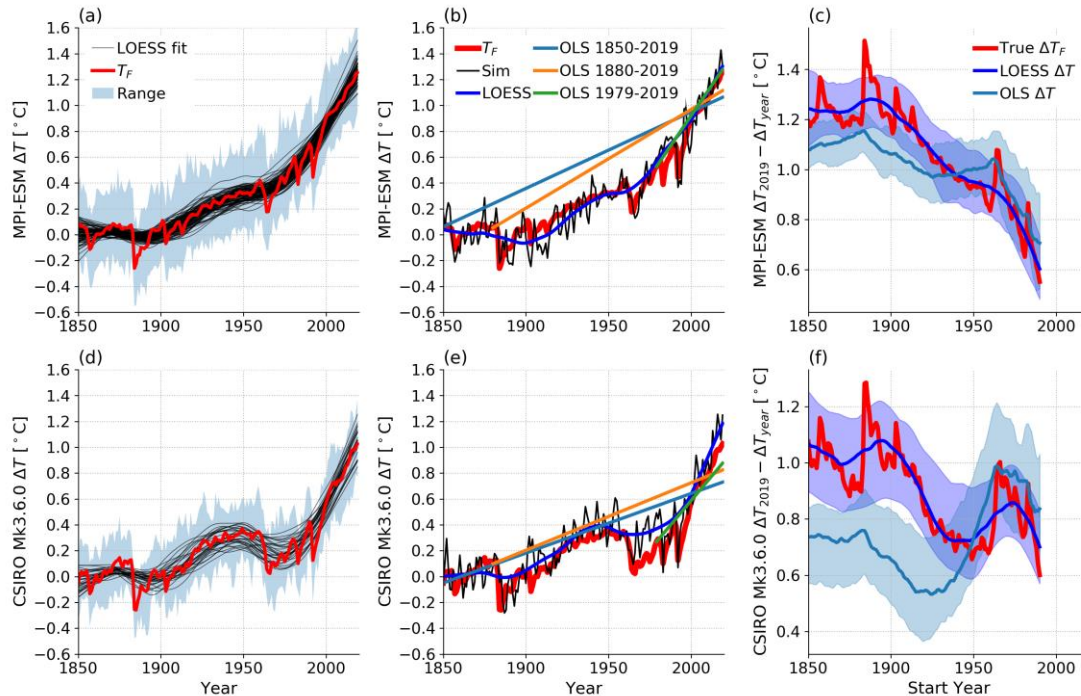
493 Global_3 $\text{LOESS}_{\text{bsln}}$ ΔGMST to 2019 is our main input for subsequent analysis such as
 494 remaining carbon budget, for which combined 17–83 % uncertainty is required; recalculating
 495 the combined uncertainty following Section 2.2.4 yields 1.14°C [1.05 – 1.25].

496
 497 **3.2 Large Ensemble Validation**
 498

499 Figure 4(a,d) shows the MPI-GE and CSIRO Mk3.6.0 annual SAT range, individual LOESS_{md}
 500 fits and GMST_F estimate, Figure 4(b,e) contains example LOESS and OLS fits to a single
 501 simulation and Figure 4(c,f) shows the forced, LOESS and OLS ΔGMST estimates through 2019
 502 for each start year from 1850–1980.

503 The ΔGMST_F and LOESS ΔGMST agree well outside of periodic ΔGMST_F spikes from volcanic
 504 eruptions, i.e. when the forced change is smooth over our ± 20 year window, such that
 505 $\Delta\text{GMST}_{\text{LOESS}} \approx \Delta\text{GMST}_F$. OLS is biased relative to ΔGMST_F in the long term, and is more
 506 sensitive to internal variability in the short term, e.g. for 1990–2019 OLS ensemble spread is 62
 507 % (MPI-ESM) or 26 % (CSIRO Mk3.6.0.) larger than LOESS ensemble spread.

508
 509



510
 511 **Figure 4.** (a) MPI-GE SAT outputs, full ensemble range is shaded, each simulation's LOESS fit is in grey and the
 512 ensemble mean (our estimate of GMST_F) is in red. (b) example of fits applied to a single simulation (black)
 513 including LOESS (dark blue) and OLS over three different periods (straight lines) with GMST_F in red. OLS lines are
 514 shifted up so that their end points correspond to the relevant ΔGMST for ease of comparison. (c) calculated ΔGMST
 515 for GMST_F (red), based on the LOESS fit (dark blue) and based on OLS (cyan). For the fits, the lines are the
 516 ensemble median and the shaded regions the 5—95 % range. (d—f) as (a—c) but for the CSIRO Mk 3.6.0 ensemble.

517
 518 Table 3 contains the large ensemble ΔGMST estimates. For periods like 1850—1900 to 2010—
 519 2019, we use Section 2.2.2's $\text{LOESS}_{\text{bsln}}$ approach while OLS is fit between the middle of each
 520 period. In both ensembles LOESS performs similarly to the period difference with median bias
 521 magnitude <0.02 °C and an almost matching 5—95 % range. LOESS slightly outperforms
 522 centered period differences evaluated from 1850-1900 to end periods ranging from 1986-1995
 523 through 2010-2019 when validated against 30-year average (see Figure S15), This validates
 524 LOESS performance, and Table 3 shows an advantage over period means since its calculation
 525 can be extended to the latest available year without greatly inflated uncertainty. The 0.06—0.10
 526 °C discrepancies for 1880—2019 LOESS- GMST_F are likely because the LOESS window
 527 centred at 1880 captures Krakatoa's large post-1883 cooling, thereby reducing the 1880 LOESS
 528 estimate and increasing its 1880—2019 ΔGMST . These results show that such biases are period-
 529 dependent, are indeed negligible for 1850—1900 to 2019 in these models, and support our
 530 analysis of these periods.

531
 532

533 As our carbon budget calculations include an internal variability error component, we consider
 534 ensemble spread and statistical errors as candidates and compare the $\text{LOESS}_{\text{bsln}}$ ensemble 83rd
 535 minus 17th percentile and the statistical 17—83 % ranges for each run. The CSIRO Mk3.6.0
 536 ensemble spread is 0.22 °C, equal to the largest individual run uncertainty (ensemble median

537 0.17 °C), while for MPI-ESM the ensemble spread (0.11 °C) and median statistical error (0.12
 538 °C) almost match. The statistical errors are a reasonable representation of internal variability
 539 error in MPI, but underestimate that in CSIRO Mk 3.6.0. For the internal variability component
 540 of Δ GSAT uncertainty in our carbon budgets we present results both using statistical error
 541 (derived only from observational data) and a more conservative estimate using the ± 0.11 °C
 542 CSIRO Mk3.6.0 ensemble spread.

543
 544 This large ensemble analysis has:

- 545 (i) provided limited support for our LOESS-based statistical uncertainty estimates
 546 being similar to model variability,
- 547 (ii) shown that LOESS matches or exceeds period difference performance while
 548 having lower long-term bias and short-term uncertainty than OLS,
- 549 (iii) verified that LOESS reliably reproduces Δ GMST_F outside of years immediately
 550 following large volcanic eruptions, particularly supporting our LOESS_{bsln} results.

551
 552
 553
 554
 555
 556
 557
 558
 559

Table 3. Long-term Δ GMST estimated for various periods for the ensemble mean T_F , plus the ensemble medians and 5—95 % ranges for estimates based on LOESS, OLS or taking the mean of the raw SAT outputs. Uncertainties in T_F differences are derived by treating T_F as a sample mean and assuming the ensemble members follow a Gaussian distribution in any given year. The period errors are then combined in quadrature.

	MPI-ESM Δ GMST[°C] median [5—95 %] [17—83 %]		
Method	1850-1900 to 2010-2019	1850-1900 to 2019	1880 to 2019
T_F	1.15 [1.15-1.16] [1.15-1.16]	1.25 [1.23-1.28] [1.24-1.27]	1.20 [1.17-1.23] [1.18-1.22]
LOESS	1.16 [1.07-1.24] [1.11-1.21]	1.25 [1.15-1.36] [1.21-1.32]	1.26 [1.15-1.36] [1.20-1.31]
OLS	1.02 [0.93-1.12] [0.97-1.07]	1.13 [1.04-1.23] [1.08-1.18]	1.15 [1.06-1.23] [1.10-1.20]
Individual runs	1.15 [1.07-1.24] [1.11-1.20]	1.24 [1.04-1.48] [1.12-1.40]	1.20 [0.92-1.50] [1.04-1.39]
	CSIRO Mk3.6.0 Δ GMST[°C]		
T_F	0.92 [0.90-0.93] [0.91-0.92]	1.03 [0.99-1.07] [1.00-1.05]	0.93 [0.88-0.98] [0.90-0.96]
LOESS	0.93 [0.79-1.04] [0.82-1.01]	1.05 [0.89-1.18] [0.90-1.12]	1.03 [0.84-1.16] [0.91-1.10]
OLS	0.63 [0.46-0.72] [0.52-0.70]	0.73 [0.56-0.85] [0.61-0.82]	0.75 [0.58-0.87] [0.64-0.83]
Individual runs	0.91 [0.78-1.04] [0.83-1.00]	1.03 [0.81-1.22] [0.86-1.12]	0.94 [0.66-1.15] [0.76-1.05]

560

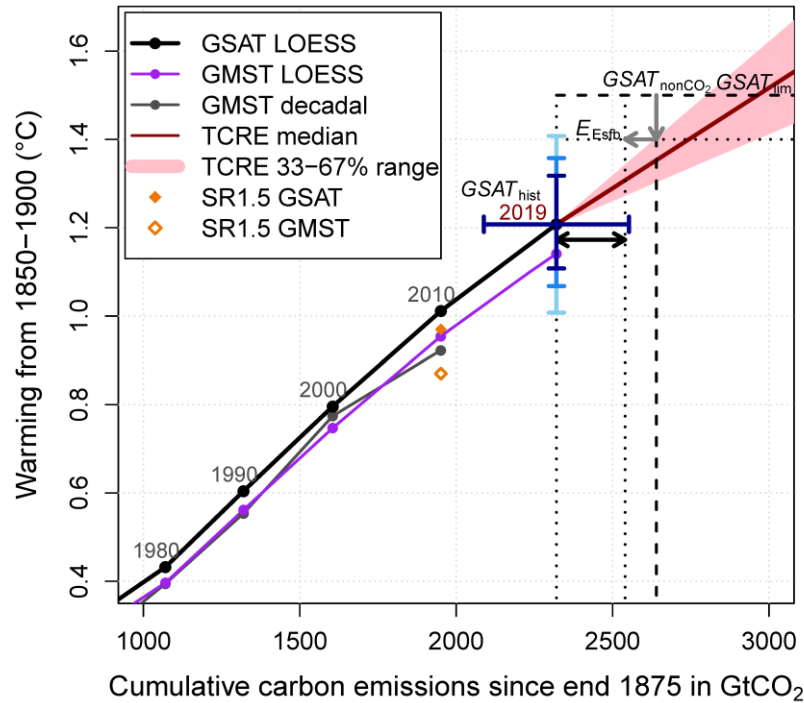
561 3.3 Global SAT estimate and Remaining Carbon Budget

562 We now convert our best estimate ΔGMST of 1.14°C [1.05 – 1.25] (17—83% uncertainty) to an
563 equivalent ΔGSAT . Our CMIP6 ensemble LOESS_{bsln} A_{blend} ratio $\Delta\text{GSAT}/\Delta\text{GMST}$ reflects an
564 increase of ΔGSAT over ΔGMST of 5.8% [4.4, 7.2] in 2014.

565 Combining this ratio and its uncertainty in quadrature with our Global_3 ΔGMST , we obtain
566 ΔGSAT of 1.21°C [1.11—1.32] from 1850—1900 to 2019, a lower uncertainty than the
567 equivalent SR1.5 estimate of $\pm 0.12^\circ\text{C}$ (Section 1.2.1.2 in Allen et al., 2018). The conservative
568 CSIRO-based internal variability yields a wider ΔGSAT range of 1.07—1.37 °C. These
569 estimates all represent uncertainty in total forced warming; however, uncertainty in
570 anthropogenic warming was estimated to be still higher at $\pm 0.2^\circ\text{C}$ (Section 1.2.1.3 in Allen et al.,
571 2018).

572 The other carbon budget calculation components also have large uncertainties. Cumulative
573 emissions to end of 2019 are 2320 ± 230 GtCO₂ (Friedlengstein et al., 2019), while non-CO₂
574 uncertainties are even higher (see Table 2.2 in Rogelj et al., 2018). Although no formal methods
575 exist to combine these uncertainties, Rogelj et al (2018) estimated overall uncertainty of $\pm 50\%$ in
576 SR1.5 remaining carbon budgets.

577 Figure 5 shows the calculation for the headline remaining carbon budget with a 66% chance to
578 stay below 1.5°C , along with the historical cumulative CO₂ emissions and temperature change.



579

580

581 **Figure 5: Global temperature change from 1850–1900 versus cumulative CO₂ emissions.** The smoothed
 582 temperature response from the Global3 blended GMST group as decadal average (blue) and LOESS_{md} trend (purple)
 583 are shown relative to cumulative CO₂ emissions from Friedlingsten et al (2019). The thick black line shows the
 584 Global3 GMST LOESS_{md} trend, adjusted by the median difference between GSAT and blended historical runs from
 585 an ensemble of 21 CMIP5 models, again relative to cumulative CO₂ emissions. The pink shaded plume and dark red
 586 line are estimated temperature response to cumulative CO₂ emissions (TCRE) from 2019 on. Also shown are other
 587 remaining carbon budget factors, T_{nonCO_2} and E_{Esfb} (gray arrows). The thick black double arrow represents the
 588 remaining carbon budget for 66% chance of remaining below 1.5°C. Vertical error bars show ΔGSAT combined
 589 observational and statistical uncertainty (dark blue), combined observational and internal variability derived from
 590 CSIRO ensemble (medium blue) and estimated uncertainty in anthropogenic warming (light blue).

591 The remaining carbon budgets from the start of 2020 for a 66% (50%) chance to stay below
 592 1.5°C and 2.0°C are 220 (350) GtCO₂ and 880 (1270) GtCO₂ respectively (rounded to nearest 5
 593 GtCO₂). Given current annual emissions of just over 40 GtCO₂, the 66% 1.5°C remaining carbon
 594 budget is only ~15 GtCO₂ lower than the equivalent carbon budgets in SR1.5 (320 GtCO₂ from
 595 2018) and Nauels et al (235 GtCO₂ from 2020). However, our 50% 1.5°C carbon budget is ~45
 596 GtCO₂ below those two studies. This follows from the slightly higher $\Delta\text{GSAT}_{\text{hist}}$ found in this
 597 study, combined with an identical TCRE spread starting in 2019 rather than a reference period
 598 centered at the start of 2011. In effect, the up-to-date estimate of $\Delta\text{GSAT}_{\text{hist}}$ reduces the
 599 contribution of TCRE uncertainty, as there is less ΔT “to go”.

600 SR1.5's secondary carbon budgets used the average ΔGMST through 2006-2015 to obtain a 66
601 % chance of staying below 1.5 °C with a budget of 470 GtCO₂ from 2018. Our alternative
602 budget using Global_3 ΔGMST instead of ΔGSAT is 305 GtCO₂ from 2020. This large
603 difference relative to SR1.5 is unsurprising as the Global_3 series show more historical warming
604 whereas SR1.5 included HadCRUT4 and its more substantial coverage bias.

605 All estimates above account for Earth system feedbacks (CO₂ and CH₄ release from warming
606 wetland and permafrost thaw) as in Rogelj et al. (2019): carbon budgets excluding this term
607 would be 100 GtCO₂ higher.

608 **4 Discussion and Conclusions**

609 We have explored the range of warming estimates since the late 19th century across different
610 observational series using multiple estimation methodologies. Our main LOESS_{bsln} Global_3
611 ΔGMST since 1850-1900 is, to our knowledge, the first such estimator that (i) integrates robust
612 statistical uncertainties, with fit residuals following the assumed noise process, (ii) has been
613 extended to provide a corresponding ΔGSAT since 1850-1900, including combined
614 observational and internal variability uncertainties, and (iii) has been validated against output
615 from model large ensembles.

616 IPCC SR1.5 reported ΔGMST of 0.87°C to 2006-2015 using four datasets (1.0°C when extended
617 to 2017) and estimated ΔGSAT of 0.97°C by adjusting one dataset (HadCRUT4) for biases
618 related to incomplete coverage and sea-air temperature differences, effectively discarding the
619 other three. The ensuing carbon budget calculation subsumed cumulative emissions up to 2017,
620 necessitating an implicit extension of ΔGSAT to that date. The simplicity and coherence of our
621 “up-to-date” ΔGMST and ΔGSAT estimates represent a clear advance over the IPCC ΔGMST
622 period difference and ΔGSAT derivation methods. Not only is LOESS_{bsln} generally an unbiased
623 ΔGMST_F estimator outside periods of volcanism, but the method includes a more consistent and
624 intuitive baseline alignment of datasets beginning in 1880 and maintains the previously stated
625 advantage of including statistical error derived using a noise model consistent with the data.
626 Moreover, validation tests with observations and the large ensembles confirm LOESS_{bsln} exhibits
627 superior performance and lower susceptibility to natural variation. None of this is surprising
628 considering that the IPCC period difference method is essentially a 10-year moving average.

629 Another key difference with IPCC SR1.5 is our consistent use of the Global_3 datasets with
630 extensive spatial interpolation. These datasets are self-evidently more representative of global
631 climate change and require smaller and less uncertain adjustments (~6%) to obtain ΔGSAT from
632 ΔGMST , in contrast to the 17% adjustment applied to HadCRUT4 in IPCC SR1.5. The Global_3
633 datasets give 0.12 °C more warming than HadCRUT4 from 1850-1900 and the divergence
634 related to incomplete coverage may well grow, as the Global_3 LOESS_{md} trend is now
635 0.03°C/decade higher than HadCRUT4's 0.17 °C/decade.

636 SR1.5 also reported 1880—2012 and 1880—2015 linear trend ΔGMST , but mainly to provide
637 “traceability” to the IPCC AR5. In contrast, AR5's main estimate of 0.85°C was based on the
638 mean linear trend of available datasets, while HadCRUT4 2003-2012 period difference from

639 1850-1900 Δ GMST estimate fed further analyses such as future projections (Collins et al., 2013)
640 and attribution (Bindoff et al., 2013).

641 If IPCC AR6 follows AR5, that would imply the three post-1850 datasets would form the basis
642 for 2010-2019 period Δ GMST relative to 1850-1900. As noted above, LOESS_{bsln} to 2019 offers a
643 superior alternative. The case for excluding HadCRUT4 is compelling, although if the
644 forthcoming HadCRUT5 represents quasi-global GMST then it should be included. Following
645 the precedent set in IPCC SR1.5, the ERSSTv5 based datasets starting 1880 should also be
646 considered, using baseline matching over 1880—1900. Our Global_3 group member, NASA
647 GISTEMP is an obvious choice for inclusion, while NOAA GlobalTemp could be excluded
648 according to our global coverage criterion. However, that case is less clear cut than
649 HadCRUT4 due to NOAA's complicated spatial coverage.

650 Since all observational datasets could be included, LOESS_{bsln} Δ GMST removes a primary
651 motivation for 1880-2019 Δ GMST in IPCC AR6. However, AR5 also compared Δ GMST trends
652 from 1880 to short-term trends from mid-century or later. Our results reinforce that 1880—2019
653 linear trend is inconsistent with LOESS_{md} 1880—2019 Δ GMST. The bias of long-term OLS
654 Δ GMST was confirmed in analysis of two large ensembles, which also showed that it has 26—
655 62 % larger uncertainty than LOESS_{md} for recent 30-year trends. As seen in Table S2, observed
656 OLS trends from 1951 have wider uncertainty than the corresponding LOESS_{md} estimates and
657 show evidence of warm bias as well (for example the NASA GISTEMP 1951—2019 OLS is
658 almost identical to 1880—2019). We therefore recommend LOESS_{md} over linear trend for both
659 long-term (> 120 years) and short-term (30-70 years) intervals.

660 LOESS_{bsln} statistical uncertainties represent another opportunity for AR6. If Δ GMST_{LOESS} is
661 close enough to Δ GMST_F then with an appropriate noise model the Δ GMST uncertainty due to
662 internal variability could be derived from the LOESS residuals. We combined this with
663 observational uncertainty and carried it forward directly to Δ GSAT for carbon budget
664 calculations, but it could also be used for other follow-on analyses. The median statistical errors
665 from the large ensemble runs are within 25% of the ensemble spreads, and the residual
666 autocorrelation structure implies potential for this approach.

667 However, models may not capture long-term internal variability. For example, recent Pacific
668 changes may indicate stronger real-world multidecadal variability (e.g. England et al., 2014),
669 although consensus is lacking (Seager et al., 2019). Substantial internal variability on ± 20 year
670 timescales or longer would result in underestimated LOESS uncertainties. By contrast, large
671 forced changes on shorter timescales, such as due to volcanism, would artificially increase the
672 uncertainties. Nevertheless, our method derives uncertainties directly from observations and so
673 may have advantages over approaches that rely on model outputs or estimated forcings (Otto et
674 al 2015; Haustein et al., 2017).

675 Given the above caveats we provided a more conservative Δ GSAT uncertainty incorporating the
676 CSIRO model large ensemble spread and its pronounced internal variability. Since our Δ GMST
677 and Δ GSAT estimates are close to observation-based anthropogenic warming, confirming a basic
678 finding of IPCC SR1.5, we treat our Δ GSAT as an estimate of Δ GSAT_{F,anthro}, albeit with
679 appropriately wider uncertainties. In general, our approach yields straightforward and up-to-date

680 estimates of Δ GMST and Δ GSAT to inform remaining carbon budget calculations that
681 incorporate appropriate Δ GSAT uncertainties .

682 To summarize, we argue strongly in favor of LOESS_{bsln} Δ GMST using series with near-global
683 coverage. Combining our statistical estimate of internal variability with dataset spread and
684 dataset parametric uncertainty results in a best estimate of warming from 1850—1900 to 2019 of
685 1.14 °C [1.05 – 1.25] (17-83% uncertainty). Not only is this updated through 2019, rather than
686 the prior-decade value of the IPCC’s period mean difference, but it includes statistical error that
687 is not derivable for period mean differences.

688 Our CMIP6-derived GSAT adjustment yields corresponding Δ GSAT of 1.21°C [1.11–1.32] (17-
689 83% uncertainty), implying a remaining carbon budget of ~220 GtCO₂ for a 67% chance that
690 Δ GSAT since 1850-1900 remains below 1.5°C. This carbon budget is ~5.5 years of current
691 emissions. Our Δ GSAT estimate uncertainty can be adapted to a desired interpretation of
692 Δ GSAT, for example, as total or anthropogenic warming. All indices can be updated annually
693 and are only dependent on the temperature datasets, yielding a set of transparent and easily
694 communicated metrics to measure progress towards climate goals.

695

696

697 **Acknowledgments and Data**

698 The authors thank Andrew Dessler for provision of MPI-GE series. DCC thanks Shaun Lovejoy
699 and Lenin Del Rio Amador for clarifying discussions.

700 MR’s contribution was carried out at the Jet Propulsion Laboratory, California Institute of
701 Technology under a contract with the National Aeronautics and Space Administration
702 (80NM0018D004).

703 Berkeley Earth data are available from <http://berkeleyearth.org/data/>. Cowtan-Way data,
704 including merged HadSST4 series, are available from [http://www-](http://www-users.york.ac.uk/~kdc3/papers/coverage2013/series.html)
705 [users.york.ac.uk/~kdc3/papers/coverage2013/series.html](http://www-users.york.ac.uk/~kdc3/papers/coverage2013/series.html). HadCRUT4 data are available from
706 <https://www.metoffice.gov.uk/hadobs/hadcrut4/data/current/download.html> . HadSST4 data are
707 available from <https://www.metoffice.gov.uk/hadobs/hadsst4/data/download.html>. NASA
708 GISTEMP data are available from <https://data.giss.nasa.gov/gistemp/>. NOAA GlobalTemp data
709 are available from [https://www.ncei.noaa.gov/data/noaa-global-surface-](https://www.ncei.noaa.gov/data/noaa-global-surface-temperature/v5/access/timeseries/)
710 [temperature/v5/access/timeseries/](https://www.ncei.noaa.gov/data/noaa-global-surface-temperature/v5/access/timeseries/). CMIP6 data are available from [https://esgf-](https://esgf-node.llnl.gov/search/cmip6/)
711 [node.llnl.gov/search/cmip6/](https://esgf-node.llnl.gov/search/cmip6/).

712

713 **References**

714 Allen, M.R., Dube, O.P., Solecki, W., Aragón-Durand, F., Cramer, W., Humphreys, S.,
715 Kainuma, M., et al. (2018). Framing and Context. In V. Masson-Delmotte, et al. (Eds.), Global
716 Warming of 1.5°C: An IPCC Special Report on the impacts of global warming of 1.5°C above
717 pre-industrial levels and related global greenhouse gas emission pathways, in the context of

- 718 strengthening the global response to the threat of climate change, sustainable development, and
 719 efforts to eradicate poverty. Intergovernmental Panel on Climate Change.
- 720 Bindoff, N.L., Stott, P.A., AchutaRao, K.M., Allen, M.R., Gillett, N., et al., 2013: Detection and
 721 Attribution of Climate Change: from Global to Regional. In: *Climate Change 2013: The Physical
 722 Science Basis. Contribution of Working Group I to the Fifth Assessment Report of the
 723 Intergovernmental Panel on Climate Change* [Stocker, T.F., Qin, D., Plattner, G.-K., Tignor, M.,
 724 Allen, S.K., et al. (Eds.)]. Cambridge University Press, Cambridge, United Kingdom and New
 725 York, NY, USA.
- 726 Brohan, P., Kennedy, J. J., Harris, I., Tett, S. F. B., & Jones, P. D. (2006). Uncertainty estimates
 727 in regional and global observed temperature changes: A new data set from 1850. *Journal of
 728 Geophysical Research*, 111(D12). <https://doi.org/10.1029/2005jd006548>
- 729 Cahill, N., Rahmstorf, S., & Parnell, A. C. (2015). Change points of global temperature.
 730 *Environmental Research Letters*, 10(8), 84002. <https://doi.org/10.1088/1748-9326/10/8/084002>
- 731 Cleveland, W. S. (1979). Robust Locally Weighted Regression and Smoothing Scatterplots.
 732 *Journal of the American Statistical Association*, 74(368), 829–836.
 733 <https://doi.org/10.1080/01621459.1979.10481038>
- 734 Cleveland, W. S., & Grosse, E. (1991). Computational methods for local regression. *Statistics
 735 and Computing*, 1(1), 47–62. <https://doi.org/10.1007/bf01890836>
- 736 Cleveland, W. S., Grosse, E., & Shyu, W. M. (1991), Local regression models. In J.M.
 737 Chambers, & T. Hastie (Eds.), *Statistical Models in S*, Wadsworth, Pacific Grove, Calif.
- 738 Collins M, et al. (2013) Long-term Climate Change: Projections, Commitments and
 739 Irreversibility. In: *Climate Change 2013: The Physical Science Basis. Contribution of Working
 740 Group I to the Fifth Assessment Report of the Intergovernmental Panel on Climate Change*, eds
 741 Stocker TF, et al. (Cambridge University Press, Cambridge, United Kingdom and New York,
 742 NY, USA).
- 743 Cowtan, K., Hausfather, Z., Hawkins, E., Jacobs, P., Mann, M. E., Miller, S. K., et al. (2015).
 744 Robust comparison of climate models with observations using blended land air and ocean sea
 745 surface temperatures. *Geophysical Research Letters*, 42(15), 6526–6534.
 746 <https://doi.org/10.1002/2015GL064888>
- 747 Cowtan, K., Jacobs, P., Thorne, P., & Wilkinson, R. (2018a). Statistical analysis of coverage
 748 error in simple global temperature estimators. *Dynamics and Statistics of the Climate System*,
 749 3(1). <https://doi.org/10.1093/climsys/dzy003>
- 750 Cowtan, K., Rohde, R., & Hausfather, Z. (2018b). Evaluating biases in sea surface temperature
 751 records using coastal weather stations. *Quarterly Journal of the Royal Meteorological Society*,
 752 144(712), 670–681. <https://doi.org/10.1002/qj.3235>

- 753 Cowtan, K., & Way, R. G. (2014a). Coverage bias in the HadCRUT4 temperature series and its
 754 impact on recent temperature trends. *Quarterly Journal of the Royal Meteorological Society*,
 755 140(683), 1935–1944. <https://doi.org/10.1002/qj.2297>
- 756 Cowtan, K., & Way, R. G. (2014b). Update to “Coverage bias in the HadCRUT4 temperature
 757 series and its impact on recent temperature trends”. *Temperature reconstruction by domain:*
 758 *version 2.0 temperature series*. <https://doi.org/10.13140/RG.2.1.4728.0727>
- 759 Deser, C., Lehner, F., Rodgers, K. B., Ault, T., Delworth, T. L., DiNezio, P. N., et al. (2020).
 760 Insights from Earth system model initial-condition large ensembles and future prospects. *Nature*
 761 *Climate Change*, 10(4), 277–286. <https://doi.org/10.1038/s41558-020-0731-2>
- 762 Dessler, A. E., Mauritsen, T., & Stevens, B. (2018). The influence of internal variability on
 763 Earth’s energy balance framework and implications for estimating climate sensitivity.
 764 *Atmospheric Chemistry and Physics*, 18(7), 5147–5155. [https://doi.org/10.5194/acp-18-5147-](https://doi.org/10.5194/acp-18-5147-2018)
 765 2018
- 766 England, M. H., McGregor, S., Spence, P., Meehl, G. A., Timmermann, A., Cai, W., et al.
 767 (2014). Recent intensification of wind-driven circulation in the Pacific and the ongoing warming
 768 hiatus. *Nature Climate Change*, 4(3), 222–227. <https://doi.org/10.1038/nclimate2106>
- 769 Eyring, V., Bony, S., Meehl, G. A., Senior, C. A., Stevens, B., Stouffer, R. J., & Taylor, K. E.
 770 (2016). Overview of the Coupled Model Intercomparison Project Phase 6 (CMIP6) experimental
 771 design and organization. *Geoscientific Model Development*, 9(5), 1937–1958.
 772 <https://doi.org/10.5194/gmd-9-1937-2016>
- 773 Flato, G., Marotzke, J., Abiodun, B., Braconnot, P., Chou, S.C., et al. (2013). Evaluation of
 774 Climate Models. In: *Climate Change 2013: The Physical Science Basis. Contribution of Working*
 775 *Group I to the Fifth Assessment Report of the Intergovernmental Panel on Climate Change*
 776 [Stocker, T.F., Qin, D., Plattner, G.-K., Tignor, M., Allen, S.K., et al. (Eds.)]. Cambridge
 777 University Press, Cambridge, United Kingdom and New York, NY, USA.
- 778 Forster, P. M., Maycock, A. C., McKenna, C. M., & Smith, C. J. (2019). Latest climate models
 779 confirm need for urgent mitigation. *Nature Climate Change*. [https://doi.org/10.1038/s41558-019-](https://doi.org/10.1038/s41558-019-0660-0)
 780 0660-0
- 781 Foster, G., & Rahmstorf, S. (2011). Global temperature evolution 1979–2010, *Environmental*
 782 *Research Letters*, 6(4), 44022. <https://doi.org/10.1088/1748-9326/6/4/044022>
- 783 Freeman, E., Woodruff, S. D., Worley, S. J., Lubker, S. J., Kent, E. C., Angel, W. E., et al.
 784 (2016). ICOADS Release 3.0: a major update to the historical marine climate record.
 785 *International Journal of Climatology*, 37(5), 2211–2232. <https://doi.org/10.1002/joc.4775>
- 786 Friedlingstein, P., Jones, M. W., O., Sullivan, M., Andrew, R. M., Hauck, J., Peters, G. P., et al.
 787 (2019). Global Carbon Budget 2019. *Earth System Science Data*, 11(4), 1783–1838.
 788 <https://doi.org/10.5194/essd-11-1783-2019>

- 789 Goodwin, P., Katavouta, A., Roussenov, V. M., Foster, G. L., Rohling, E. J., & Williams, R. G.
 790 (2018). Pathways to 1.5 °C and 2 °C warming based on observational and geological constraints.
 791 *Nature Geoscience*, 11(2), 102–107. <https://doi.org/10.1038/s41561-017-0054-8>
- 792 Hansen, J., Ruedy, R., Sato, M., Imhoff, M., Lawrence, W., Easterling, D., et al. (2001). A closer
 793 look at United States and global surface temperature change. *Journal of Geophysical Research:*
 794 *Atmospheres*, 106(D20), 23947–23963. <https://doi.org/10.1029/2001jd000354>
- 795 Hartmann, D.L., A.M.G. Klein Tank, M. Rusticucci, L.V. Alexander, S. Brönnimann, et al.,
 796 2013a: Observations: Atmosphere and Surface. In: *Climate Change 2013: The Physical Science*
 797 *Basis. Contribution of Working Group I to the Fifth Assessment Report of the Intergovernmental*
 798 *Panel on Climate Change* [Stocker, T.F., Qin, D., Plattner, G.-K., Tignor, M., Allen, S.K., at al.
 799 (Eds.)]. Cambridge University Press, Cambridge, United Kingdom and New York, NY, USA.
- 800 Hartmann, D.L., A.M.G. Klein Tank, M. Rusticucci, L. Alexander, S. Brönnimann, et al.
 801 (2013b): Observations: Atmosphere and Surface Supplementary Material. In: *Climate Change*
 802 *2013: The Physical Science Basis. Contribution of Working Group I to the Fifth Assessment*
 803 *Report of the Intergovernmental Panel on Climate Change* [Stocker, T.F., Qin, D., Plattner, G.-
 804 K., Tignor, M., Allen, S.K., at al. (Eds.)]. Cambridge University Press, Cambridge, United
 805 Kingdom and New York, NY, USA.
- 806 Hausfather, Z., Cowtan, K., Clarke, D. C., Jacobs, P., Richardson, M., & Rohde, R. (2017).
 807 Assessing recent warming using instrumentally homogeneous sea surface temperature records.
 808 *Science Advances*, 3(1), e1601207. <https://doi.org/10.1126/sciadv.1601207>.
- 809 Haustein, K., Allen, M. R., Forster, P. M., Otto, F. E. L., Mitchell, D. M., Matthews, H. D., &
 810 Frame, D. J. (2017). A real-time Global Warming Index. *Scientific Reports*, 7(1).
 811 <https://doi.org/10.1038/s41598-017-14828-5>
- 812 Hawkins, E., Burt, S., Brohan, P., Lockwood, M., Richardson, H., Roy, M., & Thomas, S.
 813 (2019). Hourly weather observations from the Scottish Highlands (1883–1904) rescued by
 814 volunteer citizen scientists. *Geoscience Data Journal*, 6(2), 160–173.
 815 <https://doi.org/10.1002/gdj3.79>
- 816 Hoegh-Guldberg, O., D. Jacob, M. Taylor, M. Bindi, S. Brown, et al., 2018: Impacts of
 817 1.5°C Global Warming on Natural and Human Systems. *Global Warming of 1.5°C. An IPCC*
 818 *Special Report on the impacts of global warming of 1.5°C above pre-industrial levels and related*
 819 *global greenhouse gas emission pathways, in the context of strengthening the global response to*
 820 *the threat of climate change, sustainable development, and efforts to eradicate poverty* [Masson-
 821 Delmotte, V., P. Zhai, H.-O. Pörtner, D. Roberts, J. Skea, P.R. Shukla, et al. (eds.)].
- 822 Huang, B., Thorne, P. W., Banzon, V. F., Boyer, T., Chepurin, G., Lawrimore, J. H., et al.
 823 (2017). Extended Reconstructed Sea Surface Temperature, Version 5 (ERSSTv5): Upgrades,
 824 Validations, and Intercomparisons. *Journal of Climate*, 30(20), 8179–8205.
 825 <https://doi.org/10.1175/jcli-d-16-0836.1>
- 826 IPCC, 2013: *Climate Change 2013: The Physical Science Basis. Contribution of Working Group*
 827 *I to the Fifth Assessment Report of the Intergovernmental Panel on Climate Change* [Stocker,

- 828 T.F., Qin, D., Plattner, G.-K., Tignor, M., Allen, S.K., et al. (Eds.). Cambridge University
829 Press, Cambridge, United Kingdom and New York, NY, USA.
- 830 IPCC, 2014: Climate Change 2014: Synthesis Report. Contribution of Working Groups I, II and
831 III to the Fifth Assessment Report of the Intergovernmental Panel on Climate Change [Core
832 Writing Team, R.K. Pachauri and L.A. Meyer (eds.)]. IPCC, Geneva, Switzerland.
- 833 Jeffrey, S. J., Rotstayn, L. D., Collier, M. A., Dravitzki, S. M., Hamalainen, C., Moeseneder, C.,
834 Wong, K. K., and J. I. Syktus (2013). Australia's CMIP5 submission using the CSIRO Mk3.6
835 model, *Australian Meteorological and Oceanographic Journal*, 63, 1–13,
836 http://www.bom.gov.au/amoj/docs/2013/jeffrey_hres.pdf
- 837 Jones, P. D., Lister, D. H., Osborn, T. J., Harpham, C., Salmon, M., & Morice, C. P. (2012).
838 Hemispheric and large-scale land-surface air temperature variations: An extensive revision and
839 an update to 2010. *Journal of Geophysical Research: Atmospheres*, 117(D5), n/a-n/a.
840 <https://doi.org/10.1029/2011jd017139>
- 841 Kennedy, J. J., Rayner, N. A., Smith, R. O., Parker, D. E., & Saunby, M. (2011). Reassessing
842 biases and other uncertainties in sea surface temperature observations measured in situ since
843 1850: 1. Measurement and sampling uncertainties. *Journal of Geophysical Research*, 116(D14).
844 <https://doi.org/10.1029/2010jd015218>
- 845 Kennedy, J. J., Rayner, N. A., Smith, R. O., Parker, D. E., & Saunby, M. (2011). Reassessing
846 biases and other uncertainties in sea surface temperature observations measured in situ since
847 1850: 2. Biases and homogenization. *Journal of Geophysical Research*, 116(D14).
848 <https://doi.org/10.1029/2010jd015220>
- 849 Lenssen, N. J. L., Schmidt, G. A., Hansen, J. E., Menne, M. J., Persin, A., Ruedy, R., & Zyss, D.
850 (2019). Improvements in the GISTEMP Uncertainty Model. *Journal of Geophysical Research:*
851 *Atmospheres*, 124(12), 6307–6326. <https://doi.org/10.1029/2018JD02952>.
- 852 Maher, N., Milinski, S., Suarez-Gutierrez, L., Botzet, M., Dobrynin, M., Kornblueh, L., et al.
853 (2019). The Max Planck Institute Grand Ensemble: Enabling the Exploration of Climate System
854 Variability. *Journal of Advances in Modeling Earth Systems*, 11(7), 2050–2069.
855 <https://doi.org/10.1029/2019ms001639>
- 856 Menne, M. J., Williams, C. N., Gleason, B. E., Rennie, J. J., & Lawrimore, J. H. (2018). The
857 Global Historical Climatology Network Monthly Temperature Dataset, Version 4. *Journal of*
858 *Climate*, 31(24), 9835–9854. <https://doi.org/10.1175/jcli-d-18-0094.1>
- 859 Morice, C. P., Kennedy, J. J., Rayner, N. A., & Jones, P. D. (2012). Quantifying uncertainties in
860 global and regional temperature change using an ensemble of observational estimates: The
861 HadCRUT4 data set. *Journal of Geophysical Research: Atmospheres*, 117(D8).
862 <https://doi.org/10.1029/2011jd017187>
- 863 Mudelsee, M. (2019). Trend analysis of climate time series: A review of methods. *Earth-Science*
864 *Reviews*, 190, 310–322. <https://doi.org/10.1016/j.earscirev.2018.12.005>

- 865 Nauels, A., Rosen, D., Mauritsen, T., Maycock, A., McKenna, C., Roegli, J., et al. (2019). ZERO
 866 IN ON the remaining carbon budget and decadal warming rates. The CONSTRAIN Project
 867 Annual Report 2019. University of Leeds. <https://doi.org/10.5518/100/20>
- 868 Nychka, D., Buchberger, R., Wigley, T. M. L., Santer, B. D., Taylor, K. E., & Jones, R. (2000).
 869 Confidence intervals for trend estimates with autocorrelated observations. NCAR manuscript.
 870 <https://opensky.ucar.edu/islandora/object/manuscripts:881>
- 871 Peng-Fei, L., F. Xiao-Li, & L. Juan-Juan (2015), Historical Trends in Surface Air Temperature
 872 Estimated by Ensemble Empirical Mode Decomposition and Least Squares Linear Fitting,
 873 Atmospheric and Oceanic Science Letters: 8:1, 10-16. <https://doi.org/10.3878/AOSL20140064>
- 874 Rahmstorf, S., Foster, G., & Cahill, N. (2017). Global temperature evolution: recent trends and
 875 some pitfalls. Environmental Research Letters, 12(5), 54001. <https://doi.org/10.1088/1748-9326/aa6825>
- 877 Richardson, M., Cowtan, K., & Millar, R. J. (2018). Global temperature definition affects
 878 achievement of long-term climate goals. Environmental Research Letters, 13(5), 54004.
 879 <https://doi.org/10.1088/1748-9326/aab305>
- 880 Rogelj, J., Shindell, D., Jiang, K., Fifita, S., Forster, P., Ginzburg, V., et al., 2018: Mitigation
 881 Pathways Compatible with 1.5°C in the Context of Sustainable Development. In: Global
 882 Warming of 1.5°C. An IPCC Special Report on the impacts of global warming of 1.5°C above
 883 pre-industrial levels and related global greenhouse gas emission pathways, in the context of
 884 strengthening the global response to the threat of climate change, sustainable development, and
 885 efforts to eradicate poverty [Masson-Delmotte, V., P. Zhai, H.-O. Pörtner, D. Roberts, J. Skea,
 886 P.R. Shukla, et al. (eds.)].
- 887 Rogelj, J., Forster, P. M., Kriegler, E., Smith, C. J., & Séférian, R. (2019). Estimating and
 888 tracking the remaining carbon budget for stringent climate targets. Nature, 571(7765), 335–342.
 889 <https://doi.org/10.1038/s41586-019-1368-z>
- 890 Risbey, J. S., Lewandowsky, S., Cowtan, K., Oreskes, N., Rahmstorf, S., Jokimäki, A., & Foster,
 891 G. (2018). A fluctuation in surface temperature in historical context: reassessment and
 892 retrospective on the evidence. Environmental Research Letters, 13(12), 123008.
 893 <https://doi.org/10.1088/1748-9326/aaf342>
- 894 Rohde, R., Muller, R.A., Jacobsen, R., Muller, E., Perlmutter, C., et al. (2013). A New Estimate
 895 of the Average Earth Surface Land Temperature Spanning 1753 to 2011. Geoinformatics &
 896 Geostatistics: An Overview, 1(1). <https://doi.org/10.4172/2327-4581.1000101>
- 897 Rotstayn, L. D., Jeffrey, S. J., Collier, M. A., Dravitzki, S. M., Hirst, A. C., Syktus, J. I., &
 898 Wong, K. K. (2012). Aerosol- and greenhouse gas-induced changes in summer rainfall and
 899 circulation in the Australasian region: a study using single-forcing climate simulations.
 900 Atmospheric Chemistry and Physics, 12(14), 6377–6404. [https://doi.org/10.5194/acp-12-6377-](https://doi.org/10.5194/acp-12-6377-2012)
 901 2012

- 902 Santer, B. D., Thorne, P. W., Haimberger, L., Taylor, K. E., Wigley, T. M. L., Lanzante, J. R., et
903 al. (2008). Consistency of modelled and observed temperature trends in the tropical troposphere.
904 *International Journal of Climatology*, 28(13), 1703–1722. [https://doi.org/ 10.1002/joc.1756](https://doi.org/10.1002/joc.1756)
- 905 Seager, R., Cane, M., Henderson, N., Lee, D.-E., Abernathy, R., & Zhang, H. (2019).
906 Strengthening tropical Pacific zonal sea surface temperature gradient consistent with rising
907 greenhouse gases. *Nature Climate Change*, 9(7), 517–522. <https://doi.org/10.1038/s41558-019-0505-x>
- 909 Smith, T.M., and R.W. Reynolds, 2005: A global merged land and sea surface temperature
910 reconstruction based on historical observations (1880–1997). *J. Clim.*, 18, 2021–2036
- 911 Susskind, J., Schmidt, G. A., Lee, J. N., & Iredell, L. (2019). Recent global warming as
912 confirmed by AIRS. *Environmental Research Letters*, 14(4), 44030.
913 <https://doi.org/10.1088/1748-9326/aafd4e>
- 914 Trenberth, K.E., Jones, P.D., Ambenje, P., Bojariu, R., Easterling, D., et al., 2007: Observations:
915 Surface and Atmospheric Climate Change. In: *Climate Change 2007: The Physical Science*
916 *Basis. Contribution of Working Group I to the Fourth Assessment Report of the*
917 *Intergovernmental Panel on Climate Change* [Solomon, S., Qin, D., Manning, M., Chen, Z.,
918 Marquis, M., et al. (eds.)]. Cambridge University Press, Cambridge, United Kingdom and New
919 York, NY, USA.
- 920 UNFCCC, 2015, Report on the Structured Expert Dialogue on the 2013–2015 Review
921 FCCC/SB/2015/INF.1
- 922 Takahashi, H., Lebsock, M. D., Richardson, M., Marchand, R., & Kay, J. E. (2019). When Will
923 Spaceborne Cloud Radar Detect Upward Shifts in Cloud Heights? *Journal of Geophysical*
924 *Research: Atmospheres*. <https://doi.org/10.1029/2018jd030242>
- 925 Visser, H., Dangendorf, S., van Vuuren, D. P., Bregman, B., & Petersen, A. C. (2018). Signal
926 detection in global mean temperatures after “Paris”: an uncertainty and sensitivity analysis.
927 *Climate of the Past*, 14(2), 139–155. <https://doi.org/10.5194/cp-14-139-2018>
- 928 Zhang, H.-M., Lawrimore, J., Huang, B., Menne, M., Yin, X., Sanchez-Lugo, A., Gleason, B.E.,
929 et al. (2019). Updated Temperature Data Give a Sharper View of Climate Trends. *Eos*, 100.
930 <https://doi.org/10.1029/2019eo128229>

931 **(c) 2020. All Rights Reserved**